LBNL-56401
HIFAN-1371

Comparison of experimental data and 3D simulations of ion beam neutralization from the Neutralized Transport Experiment

C. Thoma, D.R. Welch,
S.S. Yu, E. Henestroza, P.K. Roy, S. Eylon,
E.P. Gilson

September 22, 2004

Abstract

The Neutralized Transport Experiment(NTX) at Lawrence Berkeley National Laboratory has been designed to study the final focus and neutralization of high perveance ion beams for applications in heavy ion fusion (HIF) and high energy density physics (HEDP) experiments. Pre-formed plasmas in the last meter before the target of the scaled experiment provide a source of electrons which neutralize the ion current and prevent the space-charge induced spreading of the beam spot. NTX physics issues are discussed and experimental data is analyzed and compared with 3D particle-in-cell simulations. Along with detailed target images, 4D phase-space data of the NTX at the entrance of the neutralization region has been acquired. This data is used to provide a more accurate beam distribution with which to initialize the simulation. Previous treatments have used various idealized beam distributions which lack the detailed features of the experimental ion beam images. Simulation results are compared with NTX experimental measurements for 250 keV K^+ ion beams with dimensionless perveance of 1-7x10^{-4}. In both simulation and experiment, the deduced beam charge neutralization is close to the predicted maximum value.

1 Introduction

In the neutralized ballistic transport (NBT) scheme [1, 2, 3, 4, 5, 6, 7, 8] for heavy ion fusion (HIF), intense ion beams drift for several meters [9] after the

final focus magnet through the reactor chamber to an inertial confinement fusion (ICF) target [10]. Another application for NBT is to focus heavy ion beams onto targets for high energy density physics (HEDP) experiments. To reach the regimes of interest, the beams must focus to a spot size of 1-5 mm. For high perveance beams, in which the space charge tends to blow up the spot size, this focusing requires significant neutralization of the beam space charge [11]. The Neutralized Transport Experiment at Lawrence Berkeley National Laboratory [12, 13, 14] has been designed to study the final focus and neutralization of high perveance ion beams and to validate theoretical and simulation models [14] for driver scale transport.

An analytic estimate [11] places an upper limit on beam perveance for vacuum ballistic transport to mm spot sizes of $K \sim 10^{-5}$. Perveance, a dimensionless quantity somewhat loosely defined as the ratio of the beam potential and kinetic energy, is given by

$$K = \frac{2eZI_b}{\beta_i^3 \gamma_i^3 c^3 m_i},$$

where I_b is the (singly-stripped) ion beam current. Also Z, $\beta_i c$, m_i, and γ_i are the beam charge state, velocity, mass, and relativistic factor, respectively. For economic reasons, recent HIF designs (Robust Point Design) which have sought to reduce the number of ion beams and to increase the beam perveance to values of up to several times 10^{-4}, well above the vacuum transport cutoff. For such high perveance beams additional neutralization is required.

Since both the beam envelope and neutralization scale primarily with perveance [15], it is possible to scale the experiment to lower mass ions and particle energy as well as physical size while still preserving transverse dynamics [16] and neutralization physics. Several driver scale issues cannot be addressed in a small experiment. Most notably, since cross sections for processes such as beam stripping and collisional ionization of background gas are stongly dependent on energy, collisional processes cannot be modeled on a small scale. High current effects are also absent.

In the NTX experiment a low emittance K^+ ion beam is focused outside the neutralization region and passes through a 10-cm-long Al plasma produced by a pulsed cathode arc source just downstream from the final focus magnet. This plasma acts as an initial neutralization source of neutralizing electrons that become entrained downstream with the propagating beam. A second plasma is produced near the focus ($\sim$ 1 m downstream of the final focus magnet) by a pulsed radio frequency source to simulate the effect of the photo-ionized plasma produced by the heating of the ICF target in the chamber. This volume plasma near the beam waist provides additional neutralization of the beam. Characterization of both plasma sources suggests

that a sufficient reservoir of electrons exists to neutralize the NTX beam.

Preliminary simulations of the NTX experiment have been performed utilizing the electromagnetic particle-in-cell (PIC) code LSP [17, 8, 18]. With the LSP simulations initialized by an idealized particle distribution or one extracted from the Warp PIC code, used to simulate transport through the magnetic quadrupole lattice [19], there is general agreement between the measured focal spot and simulation result [20]. A more careful comparison of density profiles at the nominal focus shows qualitative differences. Notably, the experimental profile has a significant amount of charge in a halo extending past the beam core [14]. This feature is absent from prior LSP simulations. To determine the effect of this difference, it is essential to initialize the simulation with more realistic phase-space distribution. To this end the four dimensional transverse phase-space of the NTX beam is measured just upstream of the plasma sources. This phase-space data is used to initialize a new series of 3D LSP simulations to study the neutralization physics of the NTX experiments and to assess the agreement between experiment and simulation results.

Two previous papers [14, 21] have reported on the experimental results from the NTX experiments. The objective of the present paper is to provide quantitative comparisons of simulations and data where such is possible, and to provide qualitative insight from theory in cases where the data indicates interesting physical phenomena, but where essential details are either incomplete or not measurable in the NTX environment.

2 NTX Experiment

The neutralization section of the NTX experiment follows a series of magnetic quadrupoles which direct the beam to a focus $\sim$ 1 m downstream. The localized plasma plug is created outside the quadrupole fringe fields with a sufficient density to neutralize the ion beam (typically $n_p/Zn_b \gg 1$, where n_p and n_i are the plasma and beam densities, respectively). As the initially unneutralized ions pass through and exit the plug, plasma electrons are accelerated by the ion space charge up to the ion velocity and propagate along with the beam providing charge and current neutralization. To maintain a quasi-neutral plug region, the plasma should be in contact with a conducting boundary or large plasma region that can resupply electrons.

The volume plasma in the downstream end of the drift section provides additional neutralization to the beam. In contrast to the plasma plug, the plasma neutralization takes place locally. The axial position of the volume plasma is placed strategically in the ion trajectory to provide maximum spot size reduction, and was determined from preliminary LSP runs. The spot

size reduction with the addition of the volume plasma was predicted before the experimental results were obtained.

2.1 The NTX Beamline

The beam line consists of (a) ion beam injector, (b) 4 quadrupole magnets and (c) a meter-long final focus drift section equipped with a cathode arc plasma plug, RF plasma source, and diagnostics. Figure 1 shows a sketch of the NTX beamline.

The K^+ beam is produced within the source chamber by a standard hot-plate [22] alumino-silicate source. Pulsed power is provided by a Marx generator and a crowbar switch [23]. This Marx generator produces a pulse with 0.5–1 μs rise time and a 6-μs "flat-top". A smooth uniform bright beam profile is generated by high source temperature, smooth source surface and beam aperturing. The use of variable diameter apertures provides the experimental "knob" to vary the beam perveance. In addition, the aperture increases the beam brightness by removing the diffuse beam edge.

The beam is transported through a 2.4 m long magnetic section using four pulsed quadrupole lattices as shown in Fig. 1. The beam pipe radius, the quad length, and quad to quad spacing are 14.9 cm, 46.50 cm, and 6 cm, respectively. Field gradient and maximum field of a magnet are calculated to be 2-5 T/m and 0.6 T, respectively, with a current range of 3.3 to 8.2 kA [24]. An electron trap, 7.5 cm in radius, is located at the downstream end of the beamline, 10.16 cm from the last quadrupole lattice. A nominal negative 7 keV voltage is used across this trap for collection of stray electrons.

The final section of the beamline is known as Neutralized drift section, consisting of a cathode arc plasma plug and RF plasma source. This section is 1-m long and beam diagnostics, are installed at the end of the drift section to measure non-neutralized and neutralized beams.

Cathodic arcs are known to produce metal plasma from practically any metal of the periodic Table. If a cathodic arc plasma is used with ion extraction, the system is referred to as the "MEVVA" or "Metal Vapor Vacuum Arc, ion source". Metal plasma is generated at cathode spots, and expands rapidly, with ions attaining supersonic velocity of about 1.5×10^4 m/s. The streaming metal plasma is injected in a curved solenoid (plasma filter) to remove any liquid or solid debris particles that are produced at cathode spots, as well as neutral metal atoms. The filtered metal plasma provides the plasma plug in the current experiments.

The cathodic arc is powered by a 10-stage pulse forming network (PFN). The arc current, and thus plasma density, can be selected and tuned by the charging voltage of the PFN. For symmetry reasons, two arc sources

produce plasma in such a way that the two plasma streams enter the ion beam region from opposite directions. This MEVVA plasma plug was characterized using a Scientific Systems Langmuir probe, and aluminum plasma density was measured as a function of space and PFN charging voltage. Using the ion saturation current from the measured I-V characteristics and making simplifying assumptions about the aluminum plasma allows us to estimate the plasma density. The measurements show that the plasma density along the axis is peaked at a value of 10^{11} cm^{-3} at the location of the pair of entry ports where the plasma enters the beam line and drops off over a distance of a few centimeters.

The RF pulsed plasma source has a 6-way cross at the center of its design. A turbo-pump attached to one face maintains the vacuum, while the gas inlet and the RF quartz window are attached to the opposite face. A three-turn copper spiral antenna is situated inside a shielded box and faces the window. The RF matching network is directly connected to the antenna enclosure and is tuned to match the low impedance antenna to the 50 W transmission cable. Perpendicular to the turbo-pump and antenna, and directed into the page, are two flanges to the 6-way cross where the drift tube for the ion beam is connected. The plasma drifts into the center of the cross, and intersects the propagating ion beam. The source operates by applying a puff of argon gas and a pulse of RF power to the antenna. The potential advantages of pulsed operation are that it can easily operate at high peak RF power levels, and the amount of gas can be limited. The plasma density and the neutral gas pressure are issues primarily during the 10 μs the ion beam passes through the plasma. Consequently plasma parameters and neutral gas pressure are dynamic quantities and have been measured as a function of time in order to evaluate source operation. The gas valve and the RF power are triggered at the same time (t = 0). The source characteristics for a net forward power was $\sim$ 3.5 kW. Before t = 3.75 ms, the plasma density is less than the sensitivity of the Langmuir probe ($\sim 10^7$ cm^{-3}), and the neutral pressure is below the sensitivity of the dynamic pressure measurement (10^{-6} Torr). At t = 3.75 ms the electron density is 10^11 cm^{-3}, with simultaneous low neutral pressure.

Several diagnostics have been used to characterize the ion beam. The primary diagnostics for this experiment consist of (1) a Faraday cup, (2) a slit /slit-cup and (3) a scintillator with a gated camera system. The Faraday cup and the slit cup each consists of a collector and a guard ring (grid) with bias voltages that are controlled to collect beam ions only. In addition, we can also monitor currents flowing through the aperture plate and each of the two electron traps. The removable Faraday cup is inserted to the NTX beamline at the exit of the injector and at the end of the magnetic lattices to measure total beam current. The slit/ slit-cup arrangement is used to measure the

line-integrated beam profile (with slit cup only) and emittance (with slit and slit cup) at the same locations. Beam profile is measured optically using a glass or ceramic (96% alumina) scintillator with associated camera. Charge neutralization of this scintillator is provided by a high-transparency (80-90% transmission) metallic mesh placed on or near the surface of the scintillator. By applying a negative bias to the mesh, stray external electrons are decelerated and deflected away from the scintillator, limiting their contribution to the optical image to negligible levels. Time-resolved beam-induced images on the scintillator screen are captured with a Roper Scientific gated intensified CCD camera viewing the scintillator through a vacuum window, and images were processed using the public-domain program ImageJ.

The mapping of the four-dimensional phase-space distribution is accomplished over many shots by a scintillator-based imaging technique [14, 25, 26]. The phase-space distribution $f(x, y, x', y')$ is measured over multiple shots of the highly repeatable NTX beam. The beam cross section is scanned just downstream of the final focus magnet by a movable pinhole. The pinhole position specifies coordinates x and y. The transmitted beamlet with negligible space charge travels on an effectively ballistic trajectory to the nomimal NTX focus where it strikes the scintillator plate. The scintillator image allows extraction of x' and y' for each beamlet. The knowledge of the 4-dimensional phase space is essential in order to run more realistic simulations of the beam focusing to a small spot when drifting through neutralizing plasma.

The primary diagnostics used in the present report are beam-induced optical images captured by a CCD camera from a scintillator screen placed in the beam path at or near the expected focus. A biased metallic mesh in front of the scintillator deflects plasma and secondary electrons away from the scintillator surface and limits their contribution to the resulting optical images.

2.2 Simulation of experimental setup

LSP is used to simulate the neutralization section of the NTX experiment. The neutralization of an ion beam is investigated using an electromagnetic 3D simulation in cylindrical coordinates [27].

In order to provide a realistic simulation of the experiment, it is important to include details of the experimental setup. Besides detailed parameterization of the plasma sources and of the incoming ion beam, we must also include or at least assess the effects of the walls, the diagnostic targets, and biased plates used to control unwanted electrons. The details of the experimental setup included in the simulations are shown in Fig. 2.

The simulation space is 130 cm long and 3.8 cm in radius. Particles

are injected through an open (Neumann) boundary at $z = -30$ cm. At initialization a C^+ plasma extends from $z = -10$ to 0 cm (the experimental plasma ions are Al^+ and Al^{+2}, but ion dynamics do not play a significant role). The plasma density is cosine weighted with a maximum density of 3×10^9 cm^{-3} at $z = -5$ cm. For numerical reasons (such as the need to resolve the plasma frequency), the simulation density is taken to be an order of magnitude smaller the actual plug density. The insensitivity of simulation and experimental results and to varying plasma density values justifies this approach. The initial electron and ion temperatures are assumed to be a uniform 3 eV. Space-charge-limited emission is allowed where the plasma is in contact with the conducting wall, as well as at the $z = 100$-cm wall. This is reasonable because the plasma plug extends radially outward from the drift region. At the far endplate, electrons are produced due to ion impact.

The potential of the key electron trap just upstream of the MEVVA plasma source is used in the simulation. To prevent electrons from drifting upstream, a biased ring electrode (electron trap) is placed from $z = -19$ to -18 cm. A radial electromagnetic wave is fed into this port which gives the electrode a negative bias of 5 kV after a several-ns-long linear ramp. The volumetric plasma extends from $z = 45$ to 89 cm with a density profile obtained from the measured densities of the rf source [28] with a maximum density of 10^{10} cm^{-3}. Simulation studies again indicate that the neutralization is fairly insensitive to the details of the density distribution. A schematic illustration of the geometry and coordinate system used in the simulations is shown in Fig. 4. The weak fringe fields of the quadrupole magnet are not included. Preliminary simulations indicate that the effect of these fields on the ion beam in the simulation space is negligible.

There also an electron trap just several centimeters upstream of the scintillator to strip the ion beam of the neutralizing electrons before striking the target. A biased mesh is placed just near the surface of the scintillator to prevent electrons born in ion impact on the surface from streaming back. In general, the effect of these traps on the beam neutralization and spot size was found to be mininal in 2D simulations for $< 2 \times 10^{-4}$ perveance. Ignoring these traps allows us to place nonintercepting targets at several axial positions in the beam path near focus in a single 3D simulation.

3 Beam-plasma interactions in NTX

Various experimental results have been previously reported, in which different aspects of beam-plasma interactions were observed. In this section, we re-examine these experimental results, and will seek to provide physical insight

into the observed phenomena with the help of simulations and theory.

3.1 Partial Neutralization in "Vacuum transport"

One notable neutralization issue to emerge from the experiment is the partial neutralization of the beam in the absence of the plasma sources. A significant increase in beam spot size for vacuum transport was discovered as the beam pipe was increased in diameter from 7.7 cm to 15 cm [21]. This has been attributed to partial neutralization by secondary electrons produced by grazing collisions of halo ions with the beam pipe. As the pipe diameter is increased these collisions are reduced and secondary electron production is diminished. Electrons created at the wall of a larger beam pipe also spend less time in the path of the beam and are, therefore, less efficient at neutralizing. This effect has been artificially simulated in 2D cylindrical LSP simulations in which the pipe walls are allowed to emit a space-charge-limited supply of electrons from axial positions -10 cm to 1 m. From the simulation results, the effective beam neutralization is estimated by comparing the rms beam radius with an envelope equation in which the effective perveance is fitted to the simulation envelope. This method is described in greater detail in the subsequent sections. Neutralization fractions of 0.34 and 0.10 result from the 7.7 cm and 15 cm beam pipes respectively. The spot size for a 24 mA, 255 keV beam was found experimentally to increase by a factor of two when going to the large pipe. The simulation had a somewhat smaller increase in spot size for the same cases. When the plasma sources are on, however, they dominate the neutralization physics.

3.2 Gas effects

It is interesting that the simulations of neutralization for "vacuum transport", described in above section, assumes copious electron production at the wall, and yet, it was inadequate to account for the observed level of neutralization. A possible explanation is that we have ignored the effects of neutrals emitted from the wall upon ion impact. During the several microseconds of beam time, these neutrals can penetrate into the beam tube and provide additional neutralization. These effects were not modeled, nor is it possible at this point in time since we do not have adequate basic data on neutral production and/or ion-atom cross sections.

In addition to the neutrals produced at the wall, there are also neutrals produced when the MEVVA source and rf plasma source are turned on. The neutrals associated with the MEVVA are negligible since they operate typically at very low pressures.

The volume or rf plasma source developed at the Princeton Plasma Physics Laboratory (PPPL) [28] is intended to model the target plasma created in HIF applications. The source operates by injecting an Argon gas puff into the beam line and applying an rf pulse. The resulting gas pressure and plasma density are dynamic quantities. Time resolved measurements of the neutral Argon pressure and the plasma density show that for time scales on the order of one ms, the neutral pressure is of the order of a few times 10^{-6} Torr and the plasma density is about 10^{11} cm^{-3}. The cross sections for electron capture and stripping of K^+ ions by Ar atoms are of the order of 10^{-16} cm^2 [29] which gives a mean-free path for these processes on the order of 10^5 cm. Since the volume plasma extends axially for at most a few tens of cm, gas effects on the beam can be expected to be negligible at this pressure level. After this ms low pressure time window the neutral gas pressure increases by several orders of magnitude. The timing of the shots is adjusted so that the 10 μs NTX beam passes through the volume plasma region in the low pressure regime. The Ar gas is pumped from the beam pipe between shots. The temperature of the volume plasma has been measured to be between 1 and 2 eV on the beam axis.

3.3 Scaling of neutralization with MEVVA plasma density and temperature

The plasma plug is created by a pair of pulsed cathode-arc plasma sources located on each side of the beam axis. The plasma emerging from the sources is filtered through a copper coil with a 90 degree bend which removes neutrals and macro-particles from the flux of plasma injected into the beam line. This discharge geometry provides a clean fully-ionized Al plasma. The maximum plasma density is found to be of the order of 10^{11} cm^{-3} and increases as the applied voltage from the power supply is increased (the NTX density is only on the order of 10^8 as the beam approaches the plug) [14]. The density reaches its maximum value axially near the entry ports and is larger near the ports than on the axis. The on-axis density falls by a factor of 10 over an axial distance of about 5-cm. Measurements made by Langmuir probe indicate that the density can vary by about a factor of four as the source voltage is increased from 1.5 kV to its maximum value of 2.5 kV. Variations of this order are not expected to significantly affect the neutralization physics, since previous simulations have demonstrated an insensitivity to plug density as long as the plasma density remains significantly larger than the beam density (a factor of 10 is sufficient) [20]. Analysis of NTX data at a wide range of plug source voltages verifies that the beam spot size quickly levels off as the

voltage is increased.

The temperature of the plasma plug has been estimated to be on the order of 3 to 5 eV [30] depending on the applied voltage. Simulations show that neutralization is expected to be adversely affected by plasma temperature only when T_e exceeds the energy required to accelerate the electrons up to the plug velocity. For a 260 keV K^+ beam $\frac{1}{2}m_e v_i^2 \sim 7$ eV. Without a better measurement for plasma plug temperature it is difficult to assess the significance of this effect experimentally.

4 Lsp simulation of the NTX Experiment using Experimental 4D phase-space data

The 4D phase-space was obtained as described in the previous section. Figure 3 shows the configuration space projection of the 4D phase-space data at z_o for a 6 mA, 266 keV K^+ beam, and the same beam data when pushed ballistically to $z_o + 95$ cm. This figure shows a spot size on the order of 1 mm at the nominal target for perfect neutralization. Table 1 gives the beam envelope parameters calculated from the same data.

Initial ion beam PIC macroparticles for the simulation need to be sampled from the experimental phase-space data. This is done by a monte-carlo method which is discussed in detail in appendix A. The sampled particles are then injected into the simulation at an open boundary at the pinhole location.

Figure 4 shows that the position of the pinhole used in the 4D phase-space measurement is in the region of the ring electrode. This electrode serves as an electrostatic trap to keep plasma plug electrons from drifting upstream. The measured phase-space data is obtained in the absence of plasma, but for the full simulation including the plasma plug it is possible for energetic electrons to drift upstream towards the initial pinhole location due to the space charge force of the incoming beam head. For this reason it is necessary to transport the initial distribution back upstream prior to starting the simulation. Using the LSP simulation coordinates the pinhole is located at $z = -17.6$ cm. The simulation is set up to start at $z = -30$ cm. This requires running the particles at the pinhole location backwards for 12.6 cm with full space charge. To run the particles backwards, each particle has the sign of its velocity reversed. The particles are then extracted at a plane 12.6 cm upstream of the pinhole. These extracted particles then have their velocities flipped in sign again and are launched into a forward simulation which starts at $z = -30$ cm. The beam rms values for backwards

propagation were compared to envelope equation solutions (Eq. 7 with a unneutralized perveance of $K = 1.78 \times 10^{-4}$ for the 6 mA, 266 keV beam) with good agreement.

5 Comparison of experimental results and Lsp simulation using 4D phase-space data

The full 3D plasma simulations are performed in cylindrical coordinates with 8 azimuthal spokes. A nonuniform grid is used in the r and z coordinate directions to keep the number of grid points from getting prohibitively large. Near the axis $\Delta r \sim 1$ mm. $\Delta z \sim 4$ mm at the upstream open boundary, and ~ 1 cm at the downstream conducting wall. A fully electromagnetic noniterative implicit field solver is used to perform the simulations [27].

Figure 5 shows the initial on-axis density of the plasma plug and volume plasma. There is no initial transverse variation in the plasma density. The figure also shows the position of the pinhole and nominal target with respect to the plasma. Note that the ion beam must travel about 7.5 cm from the pinhole to the initial edge of the plasma plug. Of course some electrons from the plug may drift upstream before being stopped by the electrostatic trap. Such electrons will pre-neutralize the beam before it approaches the edge of the plug. All plasma species are initialized with a temperature of 3 eV. All wall emitted electrons are injected into the simulation with the same 3 eV temperature.

The required time step for the simulation is $c\Delta t \sim 0.3$ cm. This constraint is due to a Courant-like condition at the open boundary. For a simulation length of 130 cm for a 266 keV beam it is necessary to run up to about 40000 cm ($\sim$ 1300 ns) to reach a steady-state condition. Simulations were performed on a Linux cluster with $\sim$ 2.5 GHz processors with $\sim$ 1 GB of RAM. Simulations using four processors had run times on the order of 2-3 days.

Figure 6 shows a particle snapshot at steady state for a simulation with plasma plug and volume plasma present and illustrates the simulation space. In Fig. 7 particle plots are shown again at steady state. In this case the volume plasma is not present and the beam ion and plasma electron macroparticles are plotted separately. It is evident that the plug electrons are entrained by the ion beam. Note also that the lefthand edge of the plug stays well localized at $z = -10$ cm. This means that the ion beam will have to propagate the approximately 7.5 cm from the pinhole location (where the initial phase-space data was acquired) to the leading edge of the plasma plug with

negligible neutralization. The effect of this distance on the beam envelope is seen in Fig. 8. This figure shows the x and y rms values of the beam as a function of z, as calculated from particle transverse moments in LSP simulations. The pinhole location in this figure is $z = -17.6$ cm with the leading edge of the plasma plug at $z = -10$ cm. The simulation data labeled (a) shows the plots of beam x and y rms values as a function of z for a perfectly neutralized beam starting from the pinhole. This is the same data plotted already in Fig. 18. The data labeled (b) is the result of a simulation of a beam which is fully neutralized only after the leading edge of the plasma plug is reached. That is, the beam must travel for 7.5 cm with its full space charge. As discussed above, in the LSP runs, full neutralization is simulated by shutting off Lorentz forces on the PIC macroparticles. As seen in the figure, the case, in which the beam is neutralized only after reaching the plasma plug, focuses a few cm farther downstream and has a slightly larger spot size at the minimum than the fully neutralized case.

Also shown in the same figure are the rms values for full LSP simulations with (c) the plasma plug only, and with (d) the plug and volume plasma both present. Comparison of cases (c) and (d) demonstrates that the addition of the volume plasma enhances the neutralization considerably. To estimate the neutralization fraction the LSP results for x and y rms beam values are compared to solutions to the envelope equations. Eqs. 7 are solved by taking a simple axial dependence for the perveance. A constant neutralization fraction is taken for the region downstream of the plasma plug ($z \geq -10$ cm) while the full perveance is used upstream of the plug. Figure 9 shows that this simple neutralization model is in good agreement with $f = 0.82$ for the plasma plug only. Repeating this procedure with the volume plasma present we find the neutralization fraction increases to 0.95.

In Fig. 10, 2D density plots of the ion beam fluence (time-integrated current density) through the nominal target plane ($z = 77.6$ cm) are plotted for both measured data from the NTX experiment and LSP simulations. The measured data comes from scintillator images which have been described briefly above. The simulation fluence data is acquired by tracking the PIC particles which cross the target plane. The fluence data is binned on a 2D cartesian grid, not the cylindrical simulation grid. For each plot in the figure the x and y span the range from -3.5 to 3.5 mm, with the data binned into a 63×63 matrix. The fluence units are arbirtrary but note that each plot is normalized independently of the others. The top and bottom rows of the figure, labeled (1) and (2), show the measured and simulated data, respectively. Column (a) is for the case with only the plasma plug present, (b) with plug and volume plasma present, and (c) is for the fully neutralized case. The agreement between the measurement and simulation is good in all

cases. In Fig. 11, the simulation and experimental beam radius are compared over a range of axial positions. The experimental and simulated beam profiles are both well described by a core and diffuse halo. The effective beam radius r_e is defined as the average distance from the beam centroid to the locus of points with an intensity of e^{-1} times the maximum. Details concerning the calculation of r_e are given in appendix B.

It was noted above in reference to Figure 8 that the 7.5 cm of unneutralized propagation between the pinhole and the leading edge of the plasma plug has the effect of pushing the focus a few cm downstream from the nominal target position of the fully neutralized run. This can also be observed by comparing Fig. 20 with Fig. 12. Fig. 20 shows the 2D phase-space projections of ion beam particles at the target location for fully neutralized transport, while Fig. 12 shows the same for simulated transport through the plasma plug and volume plasma. Note that for fully neutralized transport, there is no noticeable slope in $x - x'$ and $y - y'$ plots. This is the expected behavior at a beam waist. By contrast, for transport through the plug and volume plasma these same phase-space projections still have a negative slope, which suggests that the beam is still converging at this position.

For the simulation with both the plug and volume plasma, fluence density plots are shown in Fig. 13 at increasing values of axial position. The fluence is plotted at $z =$ (a) 65, (b) 70, (c) 72.6, (d) 75, (e) 77.6, (f) 80, (g) 82.6, (h) 85, and (i) 90 cm. Note that the fluence plot between (g) 82.6 and (h) 85 cm assumes the approximate shape of the perfectly neutralized result (see Fig. 10 column (c)). Recall that the fully normalized result propagates with full neutralization for 95 cm, while the plasma simulation has an extra few cm of vacuum propagation. The beam begins to look more like the fully neutralized result when it is allowed to propagate a few cm farther downstream.

The effect of the value of N_p, the number of particles sampled from the phase-space distribution, on the simulation results is demonstrated in Fig. 14. This figure again shows fluence density plots in the target plane at steady state for simulations with the plug and volume plasma present. Density plots are shown for simulations with both $N_p = 10^4$ and 10^5. Although the overall agreement is good, for the smaller value of N_p the beam halo appears much less uniform and has noticeable pixel effects. This is because fewer distinct particles are sampled from the halo region, and those that are sampled are repeated as the input particles are wrapped around when the number of injected PIC particles exceeds N_p. With a larger value of N_p a greater number of distinct halo particles are sampled and are also wrapped around less frequently, yielding a smoother density distribution. The nominal value of N_p used for this report is 10^5.

As mentioned above, the nominal grid resolution for the simulations in this report have a minimum radial cell size (near the axis) of about one mm, and use eight azimuthal spokes, while the fluence density plots have use a much higher resolution cartesian grid. An *ad hoc* justification for the use of a higher resolution grid for the fluence diagnostic is as follows. As in all PIC treatments, the individual particle trajectories are gridless. Only the fields are calculated on the simulation grid. In the case of a highly neutralized beam, the effect of the fields on the particle trajectories will be small compared to the particle initial conditions, which are contained in the phase-space information. To ensure that the grid resolution is adequate, several simulations with decreased cell sizes are considered. In addition to the nominal grid, a simulation is performed with double the radial resolution and no change in the azimuthal or axial cell sizes, and a second simulation with sixteen azimuthal spokes and no change in the radial or transverse cell sizes. Lengthy run times precluded increasing the grid resolution in more than one coordinate direction at a time. Figure 15 again shows the fluence density plots for simulations with plug and volume plasma. The overall fluence plot is seen to be largely insensitive to both the doubling of the radial and azimuthal resolution. These calculations suggest that the resolution of the nominal grid is adequate to capture the major features of the neutralization physics. Simulations with increased total particle number (but with a fixed N_p) were also performed without a noticeable change in result.

6 Discussion and Conclusions

As noted first by C.L. Olson, a stationary plug can neutralize the beam only down to a minimum space charge potential of $\sim \frac{1}{2} m_e v_i^2$ (the energy required to accelerate the plug electron up to the beam velocity) [31]. That is, the neutralization fraction f is bounded by the relation

$$1 - f \geq \frac{\frac{1}{2} m_e v_i^2}{e\phi_{max}},$$

where ϕ_{max} is the maximum beam potential, which is, to within a geometric factor of order one, given by [32]

$$\phi_{max} \sim \frac{I}{I_o} \frac{mec^2}{e\beta}.$$

This yields a minimum effective perveance,

$$K(1 - f) \sim Z \frac{m_e}{m_i}, \tag{1}$$

which is independent of beam current and energy. The presence of the volume plasma located near the focus can provide additional neutralization below the trapping potential.

One motivation for the present study was to verify the plug neutralization scaling of Olson. For the 6 mA beam ($K = 1.78 \times 10^{-4}$) the effective neutralization fraction was found to be $f = 0.82$. This gives an effective perveance of $K(1-f) = 3.2 \times 10^{-5}$ which is only about a factor of two higher than minimum neutralization of $m_e/m_i = 1.4 \times 10^{-5}$ for singly stripped K ions.

In addition to the 6 mA case examined above, a series of experiments and simulations was performed with a 24 mA beam. According to the Olson scaling (Eq. 1), neutralization should be roughly independent of both current and energy. 4D phase-space data was obtained for a 24 mA, 256 keV beam K^+ beam ($K = 7.51 \times 10^{-4}$). Simulations and experimental analysis for the 24 mA case were restricted to the case without the volume plasma.

To estimate the neutralization fraction for this case we again attempted to fit the steady state x and y rms values calculated by LSP to solutions of the envelope equations using the initial conditions calculated from the 4D phase-space data. The result is a neutralization fraction of $f = 0.975$, or an effective perveance of $K(1-f) = 1.9 \times 10^{-5}$ which is very close to the minimum neutralization of $m_e/m_i = 1.4 \times 10^{-5}$. The experimental data for the higher current case had a spot size which was significantly larger than the simulations. There is a somewhat limited set of results at 24 mA, compared to the 6 mA data. For this reason it is difficult to assess whether the discrepancy is due to anomalous data or a drifting of the beam conditions from those used in the 4D phase-space measurement. Experiments are underway to obtain a self-consistent data set at the higher current.

We have demonstrated that 3D simulations of the neutralization region of the NTX experiment by the PIC code LSP can capture most of the neutralization physics of the beam-plasma interaction. We obtained good qualitative and quantitative agreement with NTX experimental measurement of beam profiles at the target when initializing the simulation with measured 4D phase-space data for a 6 mA beam. The simulations predict measured spot size well and gross features of the beam at the target at this current. Simulations at a higher current of 24 mA were found to be significantly smaller than available experimental beam images. Explanations for the discrepancy at higher current remain speculative.

Simulations at both current values with only the plasma plug present were found to be neutralized down to nearly the minimum trapping potential in agreement with Olson. In practice, the longitudinal compression of the beam and resulting electron heating prevent the neutralization from reaching its theoretical limit.

A 4D phase-space data

After some post-processing of the raw data, the NTX 4D phase-space data at the pinhole location consists of five columns of data.

$$\{x_i, y_i, x_i', y_i', s_i\}\,, \tag{2}$$

where

$$i = 1, 2, \ldots, N. \tag{3}$$

The first four columns give the phase-space coordinates of the ith data point and s_i gives the corresponding signal strength which is proportional to the intensity of the scintillator flash (signals are given in integer units with the smallest nonzero signal assigned a value of 1). For this report we used 4D phase-space data for a 6 mA, 266 keV beam and a 24 mA beam, 256 keV. Fig. 16 shows the six 2D projections of the phase-space for the 6 mA beam. The x and y data have 25 bins of width 1.4 mm. This is also the approximate pinhole size. The x' and y' data have been rebinned into 47 bins of width 1 mrad.

Assuming that the beam is perfectly neutralized (*i.e.,* force free) downstream of the pinhole the phase-space data may be trivially transported by the following transformation.

$$\begin{aligned} x_i(z) &= x_i(z_o) + (z - z_o)x_i'(z_o), \\ y_i(z) &= y_i(z_o) + (z - z_o)y_i'(z_o), \end{aligned} \tag{4}$$

where z_o is the original pinhole location. Figure 17 plots the 2D projections of the transported phase-space obtained from Eq. 4 at the nominal focus $z = z_o + 95$ cm for a fully neutralized beam. This is also the location of the scintillator at which the input data was obtained. The x and y coordinate data have 87 bins of width 0.115 mm. The x' and y' data have 47 bins of width 1 mrad.

Moments of the distribution can be calculated in the usual way.

$$\langle g(x, y, x', y') \rangle = \frac{\sum_{i=1}^{N} g(x_i, y_i, x_i', y_i') s_i}{\sum_{i=1}^{N} s_i}, \tag{5}$$

where g is an arbitrary function of the transverse phase-space coordinates. The properties of the beam envelope and emittance can be calculated from various particle moments. For example, the beam edge radius and divergence in the $y = 0$ plane are given by

$$\begin{aligned} a &= 2\sqrt{\langle x^2 \rangle - \langle x \rangle^2}, \\ a' &= \frac{4\left(\langle xx' \rangle - \langle x \rangle \langle x' \rangle\right)}{a}, \end{aligned} \tag{6}$$

with analogous equations for the edge radius and divergence in $x = 0$ plane, b and b'. Table 1 gives the beam envelope parameters calculated from the 4D phase-space data at the pinhole location z_o and when transported by 95 cm with perfect neutralization. The envelope equations for an unrotated elliptically shaped beam are given by

$$\begin{aligned} a'' - \frac{2K}{a+b} - \frac{\epsilon_x^2}{a^3} &= 0, \\ b'' - \frac{2K}{a+b} - \frac{\epsilon_y^2}{b^3} &= 0, \end{aligned} \tag{7}$$

where the prime denotes a derivative with respect to the axial coordinate. The $4\times$ rms (unnormalized) emittances are defined by

$$\begin{aligned} \epsilon_x &= 4\sqrt{\langle x^2\rangle\langle x'^2\rangle - \langle xx'\rangle^2}, \\ \epsilon_y &= 4\sqrt{\langle y^2\rangle\langle y'^2\rangle - \langle yy'\rangle^2} \end{aligned} \tag{8}$$

and the perveance K may include a neutralization fraction factor $(1 - f)$.

To sample PIC macroparticles from the 4D phase-space data the following procedure is used. A discrete probability distribution is constructed from the data in Eq. 2,

$$P_i = \frac{\sum_{j=1}^{i} s_j}{\sum_{j=1}^{N} s_j}. \tag{9}$$

Note that $P_0 = 0$, and $P_N = 1$. To select phase-space values for a PIC macroparticle from the probility distribution a random number is chosen over a uniform interval.

$$R \in [0, 1]\,. \tag{10}$$

R is then sorted into the appropriate phase-space bin. If

$$P_{i-1} \leq R < P_i, \tag{11}$$

a particle is created with phase-space coordinates x_i, y_i, x_i', and y_i'. This procedure is repeated until a desired number N_p of distinct macroparticles has been generated. N_p was taken to be 10^5 for the simulations in this report. All particles chosen in this fashion are given the same charge weight value and the same axial velocity. PIC particles are then injected into the simulation from an open boundary at the pinhole location. Each particle is given a time stamp and particles are injected during the time step in which their time stamp falls. The rate at which ions are injected into the simulation is fixed by the rate of increase of the time stamp. This same rate and the charge weight value also fix the ion beam current. If the simulation continues long

enough such that the number of injected particles reaches a multiple of N_p, the injection routine wraps around and begins with the first particle again.

To demonstrate that the particle sampling and injection procedure is reasonable, a perfectly neutralized PIC simulation is performed for the 6 mA beam. That is, the PIC particles are pushed with the Lorentz forces artificially shut off. The particles are injected into an open boundary at the pinhole location and allowed to propagate ballistically for about 1 m. The x and y rms values for the LSP simulation are plotted in Fig. 18 as a function of z. The rms values are calculated by taking the transverse moments of the PIC particles in thin axial slices. Also plotted are the solutions of the envelope equations given in Eq. 7 with perveance $K = 0$ for perfect neutralization, as well as the results of pushing the raw phase-space data as in Eq. 4. Note that the z axis has been shifted in the plots so that the pinhole location is at the origin. All three methods give the same results for the rms radii of the beam. Figs. 19 and 20 show 2-D transverse phase-space projections of LSP particles in a 1 cm axial slice at the pinhole location and at the nominal target location (95 cm downstream of pinhole). Comparison with Figs. 16 and 17 show that the PIC particles capture and accurately transport the phase-space information for the fully neutralized case.

B Calculation of effective beam radius

Determining a valid figure of merit for the beam size from scintillator images is complicated by several factors. The raw data tends to have a significant amount of pixel noise as well as background. Calculation of the rms beam radius from the raw moments of the data is very sensitive to the manner in which the background is removed from the image as well as to the tails of the distribution. The partially neutralized beams considered tend to have a relatively small core along with a large halo, with the latter dominating the rms value. For these reasons the rms beam radius (which is very useful for purposes of comparison to the envelope equation) as calculated from the image data tends not to be a good figure of merit for the beam size. In this appendix we describe a procedure for calculating an effective beam radius. Although this method was devised for analyzing the NTX scintillator images, simulation results were processed in the same manner, allowing for a direct comparison of beam sizes.

We have chosen to model the beam intensity from the image data with a weighted sum of 2D Gaussians,

$$I(x,y) = \sum_i n_i e^{-\left(\frac{x-x_i}{a_i}\right)^2 - \left(\frac{y-y_i}{b_i}\right)^2} + \text{background}, \tag{12}$$

where the parameters a_i, b_i, x_i, y_i, and n_i are determined by fitting to the image data after removal of the background. It is usually sufficient to model the background pixel values by a plane and to subtract it manually from the image. For the remainder of this treatment it is assumed that the background has been removed. By fitting the raw data to smooth analytical functions the effect of pixel noise on beam statistics is minimized.

Rather than do nonlinear curve-fitting of a large 2D data set it is convenient to fit the one dimensional lineouts

$$\begin{aligned} I_x(x) &= \int I(x,y)dy, \\ I_y(y) &= \int I(x,y)dx. \end{aligned}$$

The lineouts by virtue of being integrated in one coordinate direction are also generally less noisy than the 2D data. If the lineouts are normalized to integrate to one, the analytical lineouts are given by

$$\begin{aligned} I_x(x) &= \sqrt{\pi}\sum_i \frac{\alpha_i}{a_i} e^{-\left(\frac{x-x_i}{a_i}\right)^2}, \\ I_y(y) &= \sqrt{\pi}\sum_i \frac{\alpha_i}{b_i} e^{-\left(\frac{y-y_i}{b_i}\right)^2}, \end{aligned}$$

where

$$\alpha_i = \frac{n_i a_i b_i}{M},$$

and M is the total integrated signal. The lineouts obtained from the image data are then fitted to the analytical forms above by standard techniques for nonlinear curve fitting.

For a beam which can be well characterized by a core and halo it is natural to fit the data to two Gaussian distributions. As a further simplification it is assumed that both Gaussians are centered at the same location ($x_1 = x_2$, $y_1 = y_2$). In this case the maximum intensity of the fitted analytical function is located at the center of mass x_1, y_1. In the center of mass coordinate system the equation of the curve which has an intensity $1/e$ of the maximum is given by the equation

$$(n_1 + n_2)e^{-1} = n_1 e^{-(x/a_1)^2-(y/b_1)^2} + n_2 e^{-(x/a_2)^2-(y/b_2)^2}.$$

Converting to circular polar coordinates, this equation can be solved numerically for $r(\theta)$. The effective $1/e$ beam radius is then given by averaging over the angle theta

$$r_e = \frac{1}{2\pi}\int_0^{2\pi} d\theta r(\theta).$$

Note that the fitted parameters are obtained from the lineout data only and not the general 2D image data. Since the two lineout functions constitute a dramatic reduction of the original data set it is important to verify after the fact that the fitted 2D intensity function does indeed approximate the original image data well.

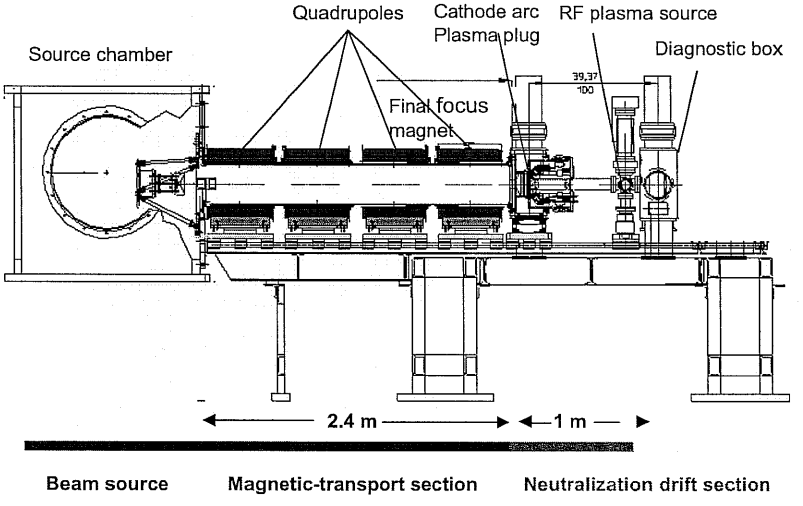

Figure 1: A sketch of the NTX beamline

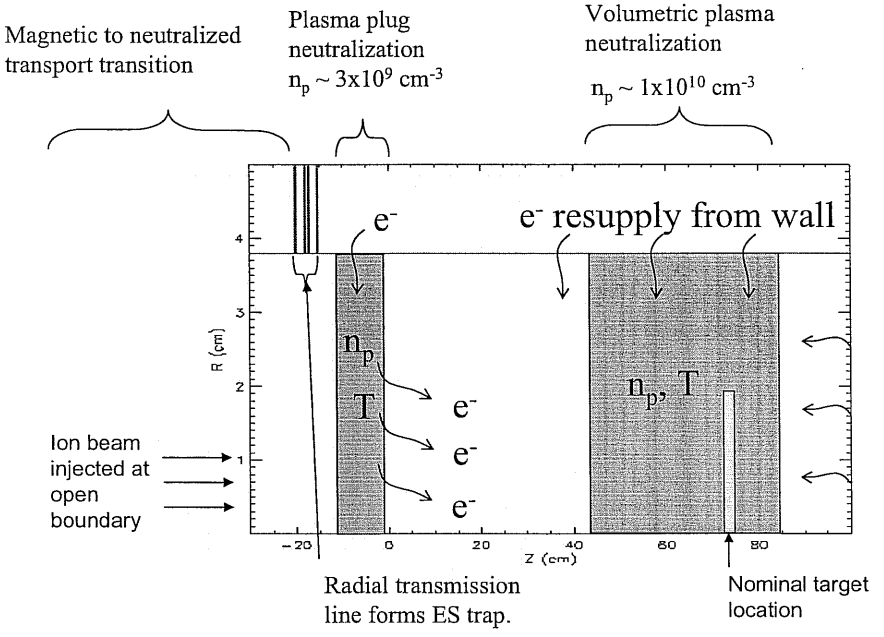

Figure 2: Schematic of geometry in LSP simulation. Magnetic quadrupoles are located upstream of the start of the simulation.

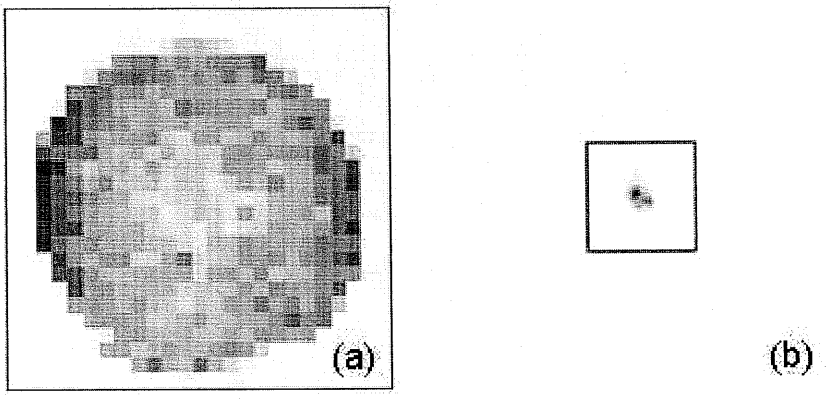

Figure 3: Configuration space density plot of NTX data for 6 mA, 266 keV K^+ beam at (a) location of pinhole z_o, and (b) location of scintillator $z_o + 95$ cm. Both plots are on the same scale. The square in (a) has a length of 35 mm and illustrates the area covered by the pinhole. The square shown in (b) illustrates the scintillator area and has a length of 10 mm.

	z_o	$z_o + 95$ cm
a (mm)	17.277	2.198
b (mm)	15.599	2.933
a' (mrad)	-17.968	0.596
b' (mrad)	-16.800	5.106
ϵ (mm-mrad)	41.594	41.594
ϵ_x (mm-mrad)	39.788	39.788
ϵ_y (mm-mrad)	49.794	49.794

Table 1: Calculation of transverse moments from 4D phase-space data for a 6 mA, 266 keV K^+ beam. Values at $z_o + 95$ cm are calculated after performing the transformations of Eq. 4 which assume perfect neutralization. Emittance values are unnormalized $4\times$ rms (see *e.g.*, Ref. [32]).

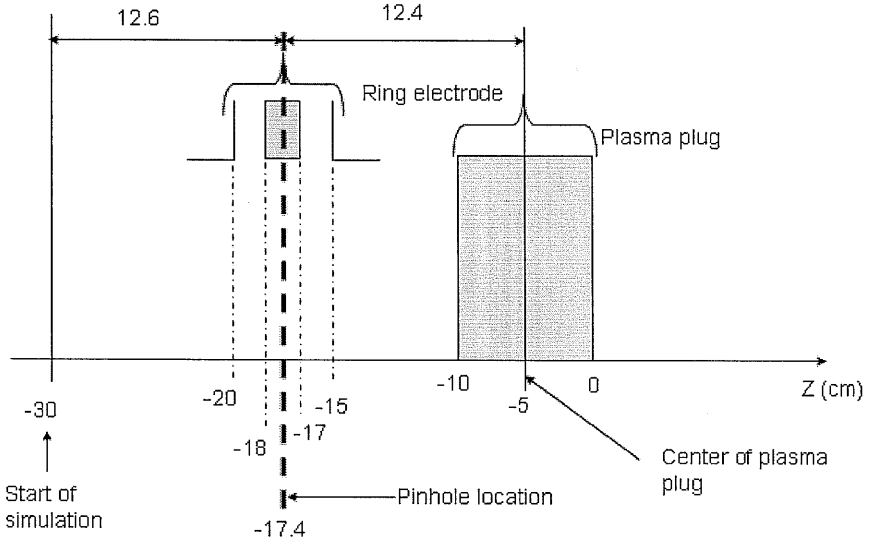

Figure 4: Closeup of geometry used in LSP simulation. Note that the 4D phase-space pinhole is in the electrostatic trap region. Magnetic quadrupoles are located upstream of the start if the simulation and the volume plasma is downstream from $z = 45$ to 89 cm.

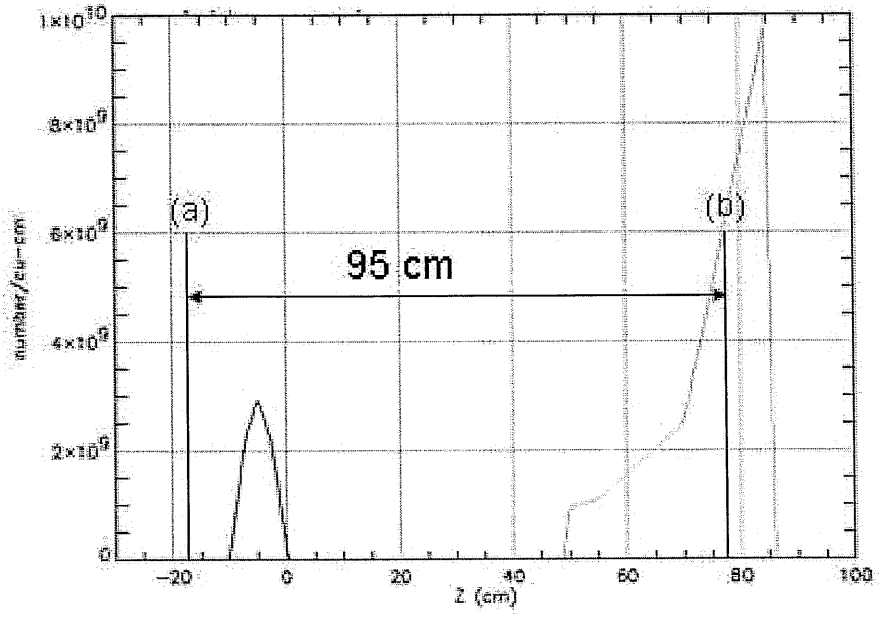

Figure 5: On-axis density profile of plasma plug (black trace) and volume plasma (red trace) at $t \sim 0$. Vertical lines labeled (a) and (b) denote the axial positions of the pinhole and nominal target, respectively.

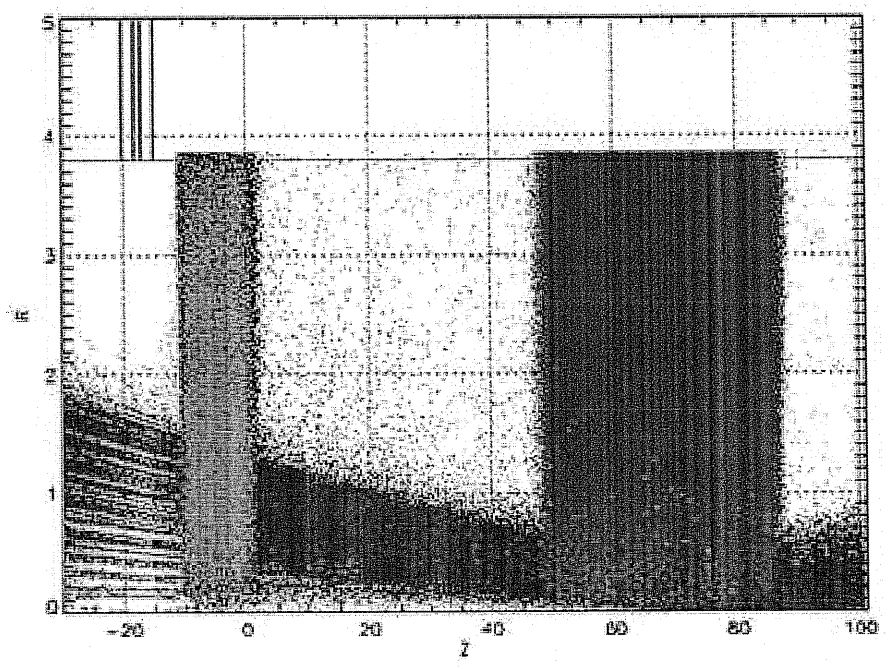

Figure 6: Particle plot of simulation of 6 mA, 266 keV K^+ beam with plasma plug and volume plasma at steady state ($t \sim 1400$ ns). Beam ions are shown in red, plasma ions in green, and electrons in red. Note that particles with all azimuthal angle values areplotted.

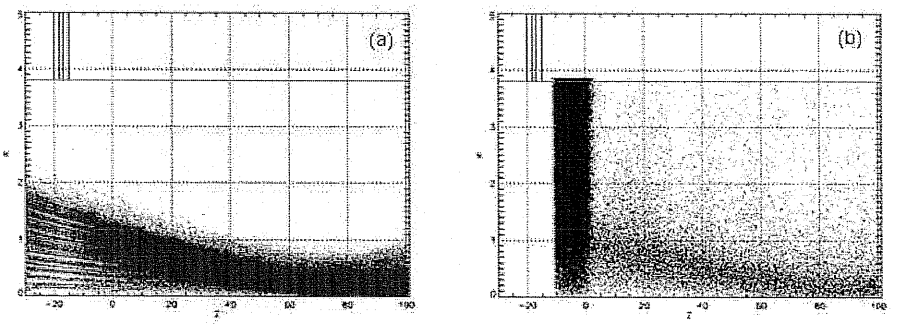

Figure 7: Particle plot of simulation of 6 mA, 266 keV K^+ beam with plasma plug only at steady state ($t \sim 1600$ ns). The plots show (a) ion beam macroparticles and (b) plasma plug electrons macroparticles.

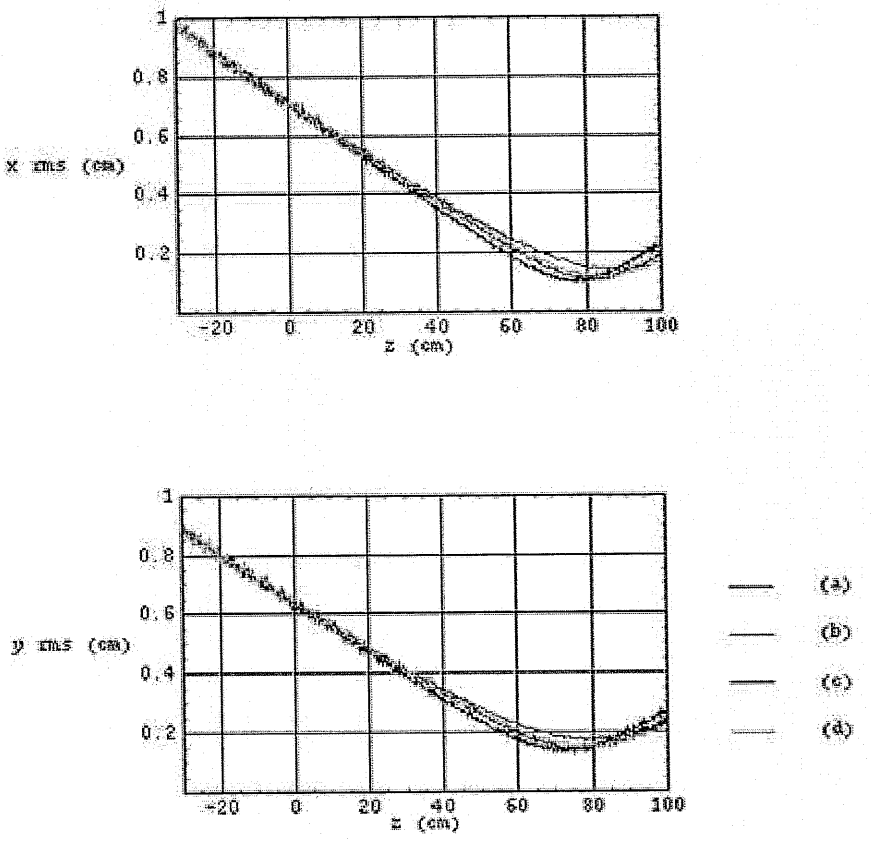

Figure 8: Plots of beam x and y rms values as a function of z for a 6 mA, 266 keV K^+ beam with (a) perfect neutralization for $z \geq -17.4$ cm (pinhole location), (b) perfect neutralization for $z \geq -10$, (c) plasma plug only present, and (d) plug and volume plasma present. All results are calculated from transverse particle moments of LSP simulations at steady state. The Lorentz forces on the particles are neglected in the appropriate axial regions of simulations (a) and (b).

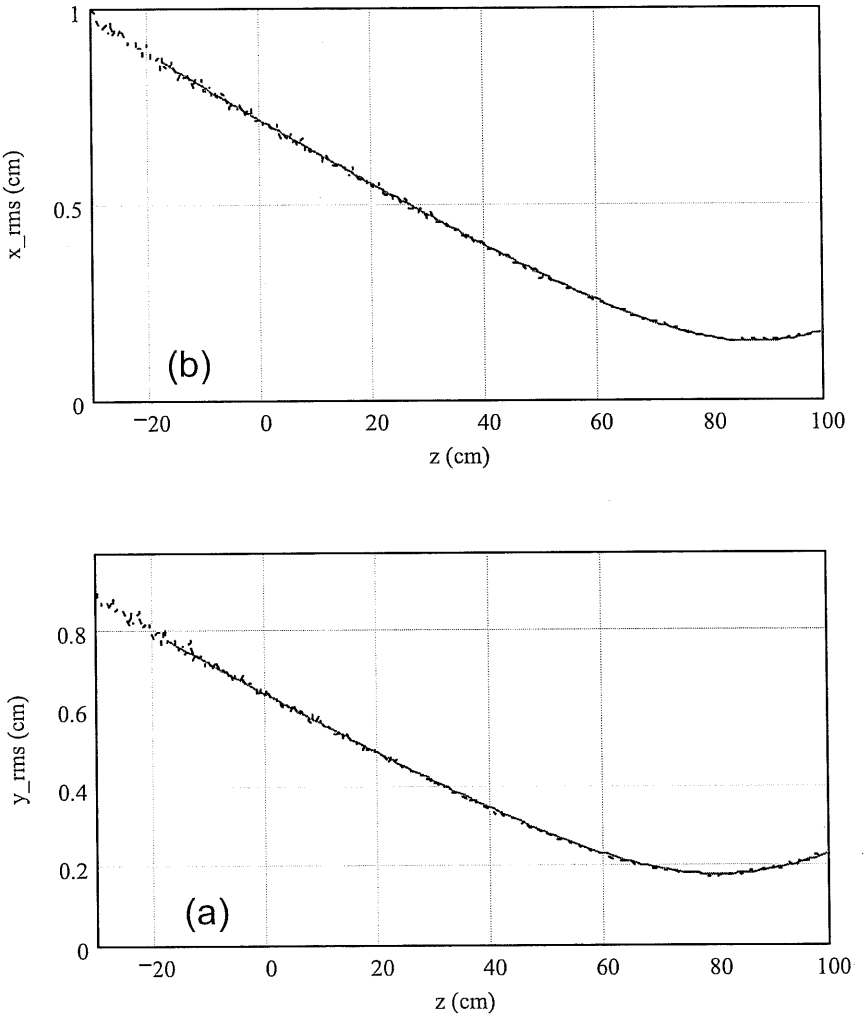

Figure 9: Plots of beam (a) x and (b) y rms values as a function of z for 6 mA beam with plasma plug only. The blue traces are the LSP results and the red traces are solutions of the envelope equations with a neutralization fraction of 0.82 in the region downstream of the plasma plug ($z \geq -10$ cm).

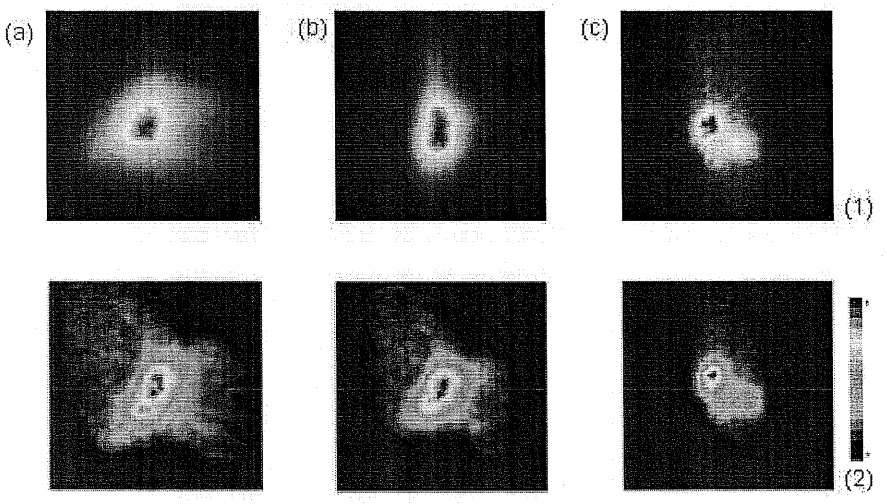

Figure 10: Density plots of fluence at steady state for NTX measurements and LSP simulations for the 6 mA, 266 keV K^+. Row (1) gives measured data, and row (2) the simulation results. Column (a) shows the results for the case with only the plasma plug, (b) plasma plug and volume plug, and (c) perfect neutralization from pinhole. In each plot the x and y axes cover the range from -3.5 to 3.5 mm. The color map is displayed in the lower right hand corner. Note that each plot is individually normalized.

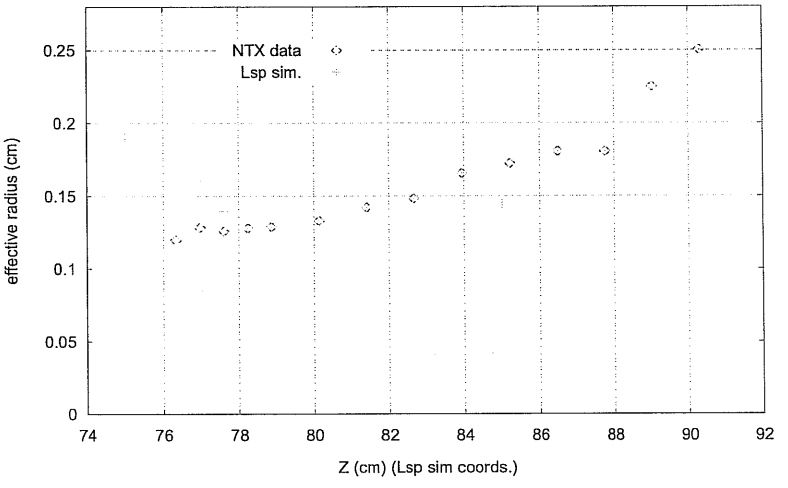

Figure 11: Comparison of effective beam radius as a function of axial position for simulation and experiment for 6 mA, 266 keV K^+ beam.

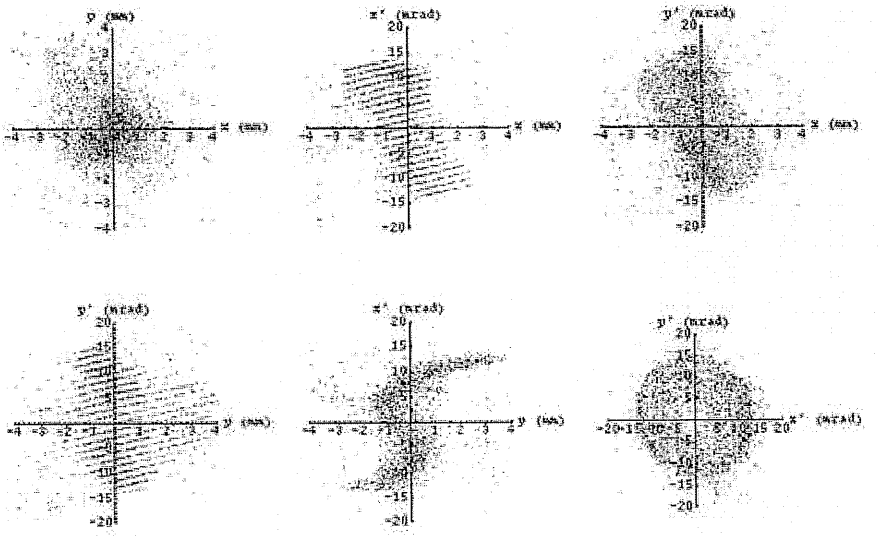

Figure 12: 2D phase-space plots of LSP particle data for 6 mA, 266 keV K^+ beam. Includes particles in 1 cm axial slice between z = [77.1, 78.1] cm. Raw data is converted from cylindrical to cartesian coordinates.

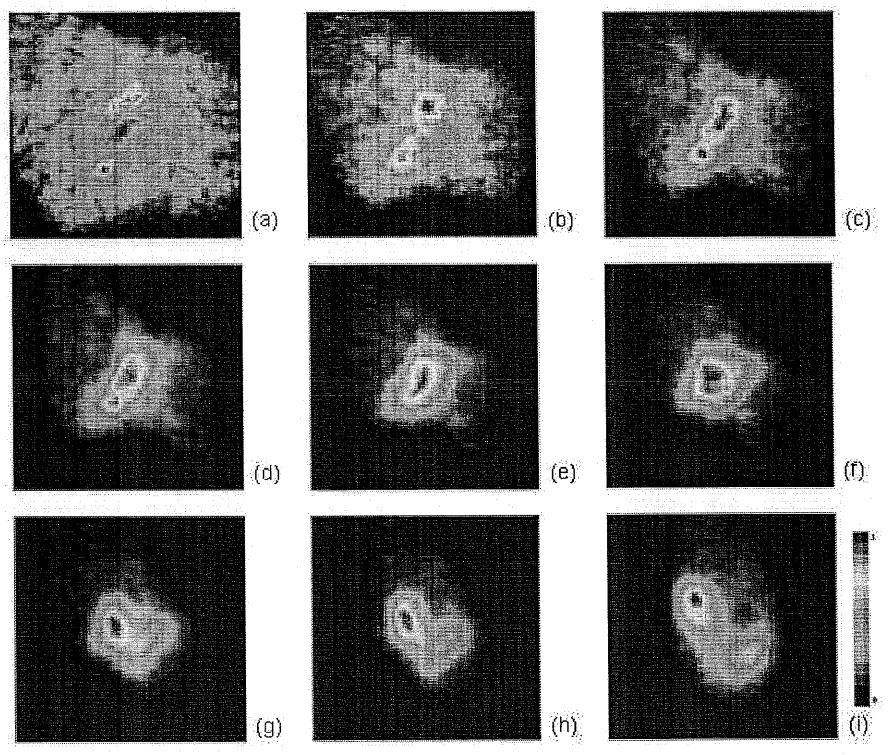

Figure 13: Density plots of fluence at steady state for an LSP simulation of 6 mA, 266 keV K^+ beam with plug and volume plasma present at increasing axial positions. z = (a) 65 cm, (b) 70 cm, (c) 72.6 cm, (d) 75 cm, (e) 77.6 cm, (f) 80 cm, (g) 82.6 cm, (h) 85 cm, and (i) 90 cm. In each plot the x and y axes cover the range from -3.5 to 3.5 mm. The color map is displayed in the lower right hand corner. Note that each plot is individually normalized.

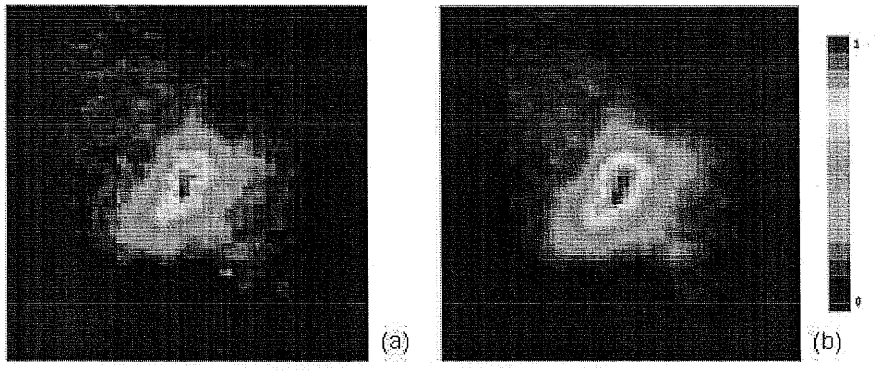

Figure 14: Density plots of fluence at the target location at steady state for an LSP simulation of the 6 mA beam with plug and volume plasma present for two different values for N_p, the number of distinct macroparticles sampled from the phase-space data. N_p = (a) 10^4, (b) 10^5. In each plot the x and y axes cover the range from -3.5 to 3.5 mm. The color map for both plots is displayed on the right. Note that each plot is individually normalized.

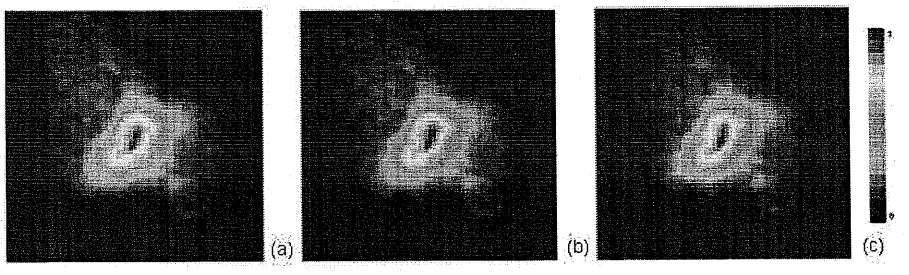

Figure 15: Density plots of fluence at the target location at steady state for LSP simulations of the 6 mA beam with varying transverse grid resolutions. (a) Nominal resolution ($(\Delta r)_{min} \sim 0.1$ mm, 8 azimuthal spokes), (b) double radial resolution, and (c) double azimuthal resolution (16 spokes). In each plot the x and y axes cover the range from -3.5 to 3.5 mm. The color map for all plots is displayed on the right. Note that each plot is individually normalized.

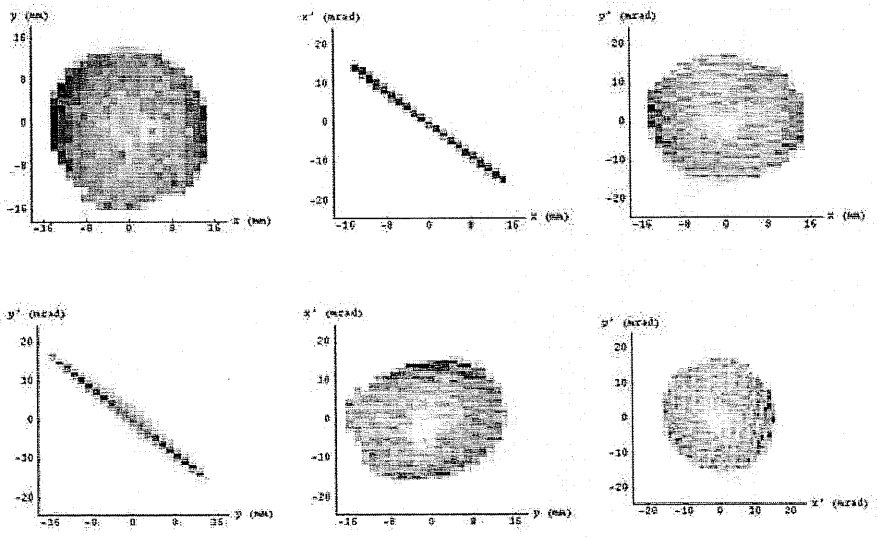

Figure 16: 2D projections of 4D phase-space data for 6 mA, 266 keV K^+ ion beam at the pinhole location z_o. The x and y coordinate data has 25 bins of width 1.4 mm. The x' and y' data have 47 bins of width 1 mrad.

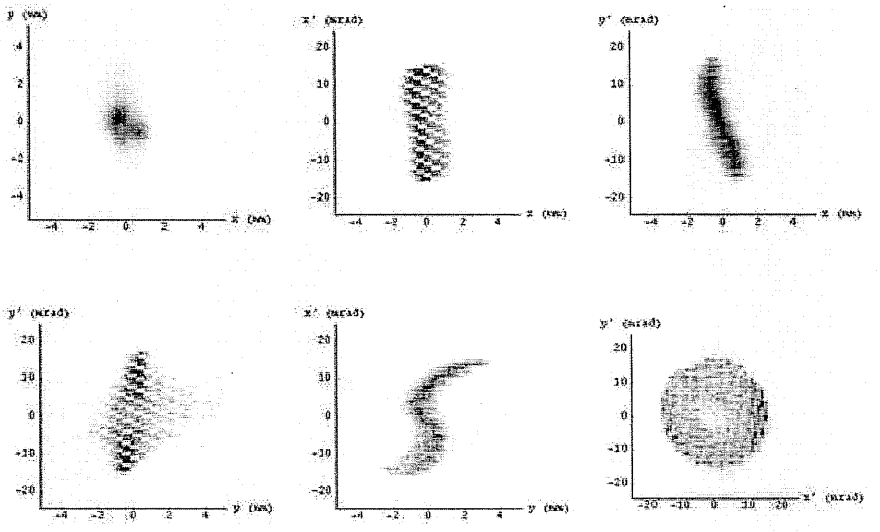

Figure 17: 2D projections of 4D phase-space data for 6 mA, 266 keV K^+ ion beam at scintillator location $z_o + 95$ cm. The x and y coordinate data has 87 bins of width 0.115 mm. The x' and y' data have 47 bins of width 1 mrad.

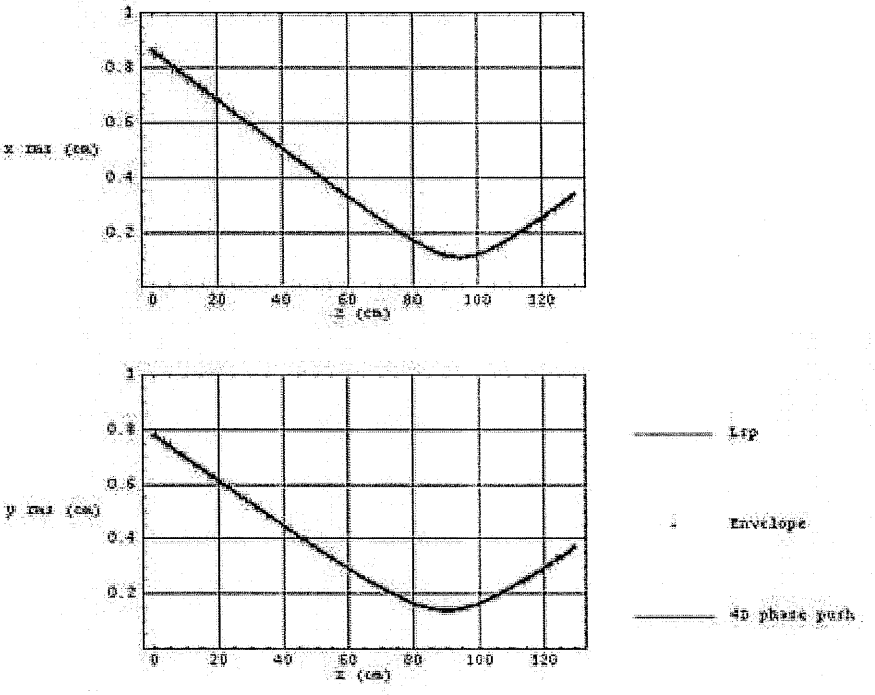

Figure 18: Plots of beam x and y rms values as a function of z for a perfectly neutralized 6 mA, 266 keV K^+ beam starting from the pinhole.

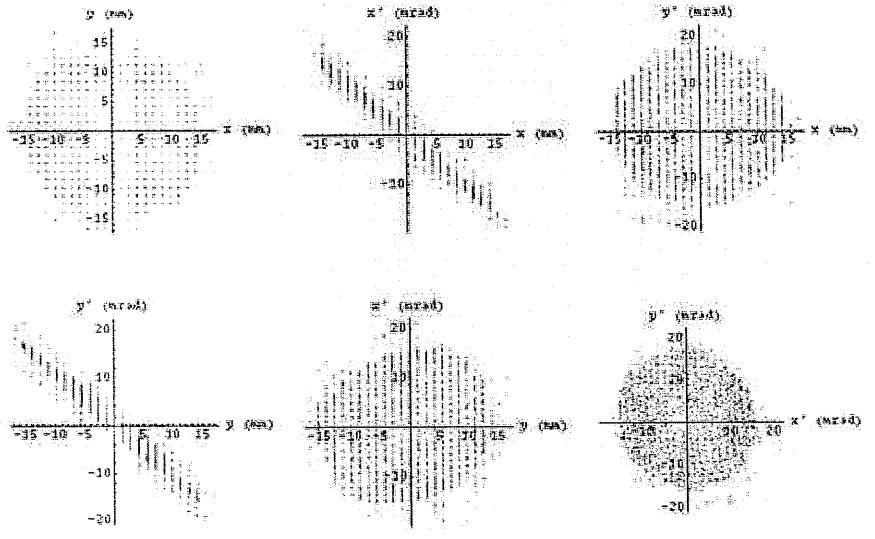

Figure 19: 2D phase-space plots of LSP particles from a 6 mA, 266 keV K^+ beam at steady state in a 1 cm axial slice in front of the pinhole. Comparison with Fig. 16 shows that the discrete particles capture the phase-space information.

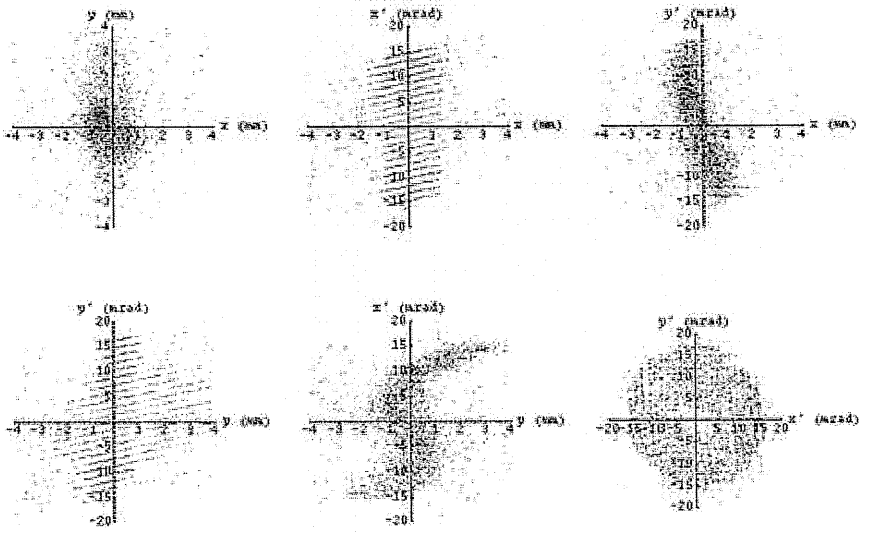

Figure 20: 2D phase-space plots of LSP particles from a 6 mA, 266 keV K^+ beam at steady state in a 1 cm axial slice in front of the nominal target (95 cm from pinhole). Comparison with Fig. 17 shows that the phase-space information has been accuarately transported by LSP.

References

[1] N. Barboza. *Fusion Eng. Des.*, 32–33:453, 1996.

[2] D.A. Callahan. *Fusion Eng. Des.*, 32–33:441, 1996.

[3] B.G. Logan and D.A. Callahan. *Nucl. Instrum. Methods Phys. Res. A*, 415:468, 1998.

[4] W.M. Sharp et al. *Bull. Am. Phys. Soc.*, 44:201, 1999.

[5] J. L. Vay. Charge compensated ion beam propagation in a reactor sized chamber. In G.H. Miley and E.M. Campbell, editors, *13th Int. Conf. on Laser Interaction and Related Plasma Phenomena, Monterey 1997*, page 267. AIP Conf. Proc. 406, 1997.

[6] I.D. Kaganovich, G. Shvets, E. Startsev, and R.C. Davison. Nonlinear charge and current neutralization of an ion beam pulse in a pre–formed plasma. *Phys. Plasmas*, 8:4180, 2001.

[7] D.V. Rose, D.R. Welch, B.V. Oliver, R.E. Clark, W.M. Sharp, and A. Friedman. Ballistic-neutralized chamber transport of intense heavy ion beams. *Nucl. Instrum. Methods Phys. Res. A*, 464:299, 2001.

[8] D.R. Welch, D.V. Rose, B.V. Oliver, R.E. Clark, W.M. Sharp, and A. Friedman. Simulation techniques for heavy ion fusion chamber transport. *Nucl. Instrum. Methods Phys. Res. A*, 464:134, 2001.

[9] S.S. Yu, W.R. Meier, R.P. Abbott, J.J. Barnard, T. Brown, D.A. Callahan, C. Debonnel, P. Heitzenroeder, J.F. Latkowski, B.G. Logan, S.J. Pemberton, P.F. Peterson, D.V. Rose, G-L. Sabbi, W.M. Sharp, and D.R. Welch. An updated point design for heavy ion fusion. *Fusion Sci. Technol.*, 44(2):266, 2003.

[10] R.O. Bangerter. *Fusion Eng. Des.*, 32–33:27, 1996.

[11] C.L. Olson. *Nucl. Instrum. Methods Phys. Res. A*, 464:118, 2001.

[12] S.S. Yu, A. Anders, F.M. Bieniosek, S. Eylon, E. Henestroza, P.K. Roy, D. Shuman, W. Waldron, W.M. Sharp, D.V. Rose, D.R. Welch, P. Efthimion, and E. Gilson. Focusing and neutralization of intense beams. In *Proceedings of the 2003 Particle Accelerator Conference*, page 98, 2003.

[13] E. Henestroza, A. Anders, S. Eylon, P.K. Roy, W. Sharp, S.S. Yu, D.V. Rose, D.R. Welch, P. Efthimion, and E. Gilson. Neutralized transport of high intensity beams. In *Proceedings of the 2003 Particle Accelerator Conference*, page 2622, 2003.

[14] E. Henestroza, S.S. Yu, A. Anders, F.M. Bieniosek, S. Eylon, W.G. Greenway, B.G. Logan, R.A. MacGill, D.B. Shuman, P.K. Roy, W.L. Waldron, D.L. Vanacek, T.L. Houck, W.M. Sharp, R.C. Davison, P.C. Efthimion, E.P. Gilson, A.B. Sefkow, D.R. Welch, and D.V. Rose. Design and characterization of a neutralized transport experiment. Submitted to *Phys. Rev. ST Accel Beams.*

[15] D.R. Welch, D.V. Rose, W.M. Sharp, and S.S. Yu. *Laser and Particle Beams*, 20:621, 2003.

[16] S.A. MacLaren, M. de Hoon, A. Faltens, W. Ghiorso, and P. Seidl. Result from the scaled final focus experiment. *Nucl. Instrum. Methods Phys. Res. A*, 464:126, 2001.

[17] T.P. Hughes, S. Yu, and R.E. Clark. Three-dimensional calculations for a 4-ka, 3.5-MV, 2-microsecond Injector with Asymmetric Power Feed. *Phys. Rev. ST Accel. Beams*, 2:110401, 1999. (`http://prst-ab.aps.org/`).

[18] LSP is a software product of Mission Research Corp. (`http://www.mrcabq.com`).

[19] E. Henestroza. In *2003 Third International Conference on Inertial Fusion Sciences and Applications*, 2003. To be published.

[20] D.R. Welch, D.V. Rose, S.S. Yu, and E. Henestroza. Simulations of ion beam neutralization in support of the neutralized transport experiment. In *2003 Third International Conference on Inertial Fusion Sciences and Applications*, 2003. To be published.

[21] P.K. Roy, S.S. Yu, E. Henestroza, A. Anders, F.M. Bieniosek, W.G. Greenway, B.G. Logan, W.L. Waldron, D.L. Vanacek, D.R. Welch, D.V. Rose, R.C. Davison, P.C. Efthimion, E.P. Gilson, A.B. Sefkow, and W.M. Sharp. Results on intense beam focusing and neutralization from the neutralized beam experiment. *Phys. Plasmas*, 11:2890, 2004.

[22] D. Baca, J.W. Kwan, and J.K. Wu. In *Proceedings of the 2003 Particle Accelerator Conference*, page 3294, 2003.

[23] W. Fawley, T. Garvey, S. Eylon, E. Henestroza, A. Faltens, T.J. Fessenden, K. Hahn, L. Smith, and D.P. Grote. *Phys. Plasmas*, 4:880, 1997.

[24] D. Shuman, S. Eylon, E. Henestroza, P.K. Roy, W. Waldron, S.S. Yu, and T. Houck. In *Proceedings of the 2003 Particle Accelerator Conference*, page 2628, 2003.

[25] F.M. Bieniosek, L. Prost, and W. Ghiorso. Beam imaging diagnostics for heavy ion beam fusion experiments. In *Proceedings of the 2003 Particle Accelerator Conference*, page 2524, 2003.

[26] A. Friedman, F.M. Bieniosek, C.M. Celata, D.P. Grote, and P.A. Seidl. Simulation using initial 4D beam particle distributions synthesized from experimental data. In *Proceedings of the 2003 Particle accelerator conference*, page 275, 2003.

[27] D.R. Welch, D.V. Rose, R.E. Clark, T.C. Genoni, and T.P. Hughes. Implementation of a non–iterative implicit electromagnetic field solver for dense plasma simulation. Presented at the 18th International Conference on Numerical Simulation of Plasmas, Sept 7–10, 2003, Falmouth, Massachussets. To appear in a special issue of *Computer Physics Communications*.

[28] P. Efthimion, E. Gilson, L. Grisham, P. Kolchin, R.C. Davison, S. Yu, and B.G. Logan. *Laser and Particle Beams*, 21:37, 2003.

[29] H.H. Lo and W.L. Fife. Electron–capture and loss cross sections for fast, heavy particles passing through gases. *Atomic Data*, 1:305, 1970.

[30] A. Anders. Ion charge state distributions of vacuum arc plasmas: The origin of species. *Phys. Rev. E*, 55:969, 1997.

[31] C.L. Olson. HIF transport issued for $p > 10^{-3}$ torr and $z > 1$. In *AIP Conference Proceedings 152*, page 215, New York, 1986. AIP.

[32] M. Reiser. *Theory and Design of Charged Particle Beams*. John Wiley & Sons, Inc., 1994.